Physica D 438 (2022) 133305

Contents lists available at ScienceDirect

Physica D

journal homepage: www.elsevier.com/locate/physd

The effect of geometry on survival and extinction in a moving-boundary problem motivated by the Fisher–KPP equation

Alexander K.Y. Tam [a,b,*], Matthew J. Simpson [b]

[a] UniSA STEM, The University of South Australia, Mawson Lakes, SA 5095, Australia
[b] School of Mathematical Sciences, Queensland University of Technology, Brisbane QLD 4000, Australia

ARTICLE INFO

Article history:
Received 20 January 2022
Received in revised form 28 March 2022
Accepted 9 April 2022
Available online 20 April 2022
Communicated by J. Garcia-Ojalvo

Keywords:
Reaction–diffusion
Fisher–Stefan
Level-set method
Spreading–vanishing dichotomy

ABSTRACT

The Fisher–Stefan model involves solving the Fisher–KPP equation on a domain whose boundary evolves according to a Stefan-like condition. The Fisher–Stefan model alleviates two practical limitations of the standard Fisher–KPP model when applied to biological invasion. First, unlike the Fisher–KPP equation, solutions to the Fisher–Stefan model have compact support, enabling one to define the interface between occupied and unoccupied regions unambiguously. Second, the Fisher–Stefan model admits solutions for which the population becomes extinct, which is not possible in the Fisher–KPP equation. Previous research showed that population survival or extinction in the Fisher–Stefan model depends on a critical length in one-dimensional Cartesian or radially-symmetric geometry. However, the survival and extinction behaviour for general two-dimensional regions remains unexplored. We combine analysis and level-set numerical simulations of the Fisher–Stefan model to investigate the survival–extinction conditions for rectangular-shaped initial conditions. We show that it is insufficient to generalise the critical length conditions to critical area in two-dimensions. Instead, knowledge of the region geometry is required to determine whether a population will survive or become extinct.

1. Introduction

The dimensionless Fisher–KPP equation,

$$\frac{\partial u}{\partial t} = \frac{\partial^2 u}{\partial x^2} + u\,(1-u)\,, \tag{1.1}$$

is a classical prototype model in mathematical biology [1–4] that describes the spatiotemporal evolution of a population density, $u(x,t) > 0$, that evolves due to linear Fickian diffusion combined with a logistic source term. A key property of the Fisher–KPP equation (1.1) is that it admits travelling-wave solutions, with long-time speed $c = 2$ for compactly-supported initial conditions, when solved on an infinite domain. By relating population invasion to travelling wave solutions, the Fisher–KPP equation and extensions of this model have been used to represent species invasion in ecology [5–8], front propagation in chemical reactions [9], and biological cell invasion [10–16]. However, despite its widespread usage, the Fisher–KPP equation has practical limitations. Firstly, any initial condition gives rise to population growth and complete colonisation. The Fisher–KPP equation is thus unsuitable for populations where extinction [17] or arrested invasion [18] is of interest. A second shortcoming is that solutions to (1.1) do not have compact support. Thus, we cannot identify the interface between occupied and unoccupied regions without ambiguity. This leads to difficulties in applying the Fisher–KPP equation to processes with well-defined invasion fronts, for example tumour cell invasion [19,20] or wound healing [11,21].

To address the shortcoming of non-compactly-supported solutions, a common approach is to modify (1.1) to incorporate degenerate nonlinear diffusion [4,22]

$$\frac{\partial u}{\partial t} = \frac{\partial}{\partial x}\left(D(u)\frac{\partial u}{\partial x}\right) + u\,(1-u)\,, \tag{1.2}$$

such that $D(0) = 0$. A common choice is $D(u) = u^k$ [22,23] for $k > 0$. Setting $k = 1$ leads to the *Porous-Fisher's* equation [22], and for $k > 1$ (1.2) is sometimes called the *generalised Porous-Fisher's* equation [21,24]. Like the Fisher–KPP equation, the generalised Porous-Fisher's equation admits travelling-wave solutions. For the minimum wave speed, these travelling waves are sharp-fronted and have compact support [25,26], thus enabling one to define an unambiguous front. However, although (1.2) admits compactly-supported travelling-waves, like the Fisher–KPP equation it guarantees population survival, and cannot be used to model population extinction or receding fronts with local decrease in density [17,18].

Another alternative to the standard Fisher–KPP equation is to consider a moving-boundary problem, such that (1.1) holds on

* Corresponding author at: School of Mathematical Sciences, Queensland University of Technology, Brisbane QLD 4000, Australia.
E-mail address: alexander.tam@qut.edu.au (A.K.Y. Tam).

https://doi.org/10.1016/j.physd.2022.133305
0167-2789/

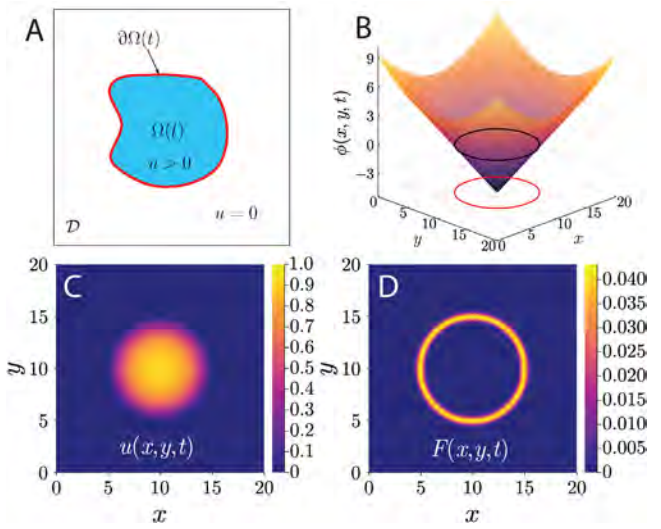

Fig. 1. Illustration of the level-set method used to solve the two-dimensional Fisher–Stefan model (2.1). (A) Schematic of the rectangular computational domain $\mathcal{D}$, which contains the blue region $\Omega(t)$ on which we solve the Fisher–KPP equation, and the red curve, which is the boundary $\partial\Omega(t)$. (B) An example level-set function, $\phi(x, y, t)$, for a disc-shaped $\Omega(t)$. The black curve is the zero level-set, and the red curve is a projection onto the (x, y) plane marked with the grid. (C) An example two-dimensional density profile $u(x, y, t)$ for a circular region. (D) An example extension velocity field $F(x, y, t)$.

a compactly-supported region $x < L(t)$, and $u(L(t), t) = 0$. The moving-boundary is assumed to evolve according to

$$\frac{\mathrm{d}L}{\mathrm{d}t} = -\kappa \frac{\partial u(L(t), t)}{\partial x}, \tag{1.3}$$

where the parameter κ relates the density gradient at $L(t)$ to the speed of the boundary. Moving-boundary problems of this type are traditionally used to model physical and industrial processes [27–31]. Indeed, the boundary condition (1.3) is analogous to the classical Stefan condition [32] for a material undergoing phase change, where κ is the inverse Stefan number. More recently, moving-boundary problems have been used to study biological and ecological phenomena, including cancer invasion, cell motility, and wound healing [8,33–38]. Usefully, reaction–diffusion moving-boundary problems often admit sharp-fronted travelling-wave solutions for a range of wave speeds [39,40]. In contrast, the travelling-wave solution to the porous-Fisher's equation is only sharp-fronted for one wave speed, the minimum wave speed [25,26]. Applying the moving-boundary problem framework to (1.1), we obtain

$$\frac{\partial u}{\partial t} = \frac{\partial^2 u}{\partial x^2} + u\,(1 - u) \quad \text{on} \quad 0 < x < L(t), \tag{1.4a}$$

$$\frac{\partial u}{\partial x} = 0 \quad \text{on} \quad x = 0, \tag{1.4b}$$

$$u = 0 \quad \text{on} \quad x = L(t), \tag{1.4c}$$

$$\frac{\mathrm{d}L}{\mathrm{d}t} = -\kappa \frac{\partial u(L(t), t)}{\partial x}, \tag{1.4d}$$

$$u(x, 0) = u_0(x) \quad \text{on} \quad 0 < x < L(0). \tag{1.4e}$$

This extension to (1.1), known as the *Fisher–Stefan* model, was first proposed by Du and Lin [41], and Du and Guo [42,43]. The Fisher–Stefan model alleviates the two practical disadvantages of Fisher–KPP, because the boundary $L(t)$ defines the front position explicitly, and it admits solutions for population extinction [41,42,44].

The Fisher–Stefan model has been studied extensively in one-dimensional Cartesian geometry. Du and Lin [41] proved that (1.4) admits solutions whereby the population density evolves to a travelling wave solution as $t \to \infty$, with asymptotic speed that depends on κ. This corresponds to population survival and successful invasion, with $u(x, t) \to 1$ as $t \to \infty$. However, Du and Lin [41] also proved that the Fisher–Stefan model admits solutions where the population fails to establish, such that $u \to 0^+$ as $t \to \infty$. This corresponds to population extinction, which cannot occur in the Fisher–KPP or generalised Porous-Fisher models. The survival–extinction behaviour of the Fisher–Stefan model depends on the critical length, $L_c = \pi/2$ [41,45]. If $L(0) > L_c$, Du and Lin [41] showed that the population will always survive. However, if $L(0) < L_c$, then survival only occurs if $L(t)$ evolves such that $L(t) > L_c$ at some time, and otherwise the population becomes extinct. In this $L(0) < L_c$ scenario, whether the solution ever attains $L(t) > L_c$ depends on the initial condition $u_0(x)$, and the parameter κ [41].

Simpson [46] extended the work of Du and Lin [41] by considering the Fisher–Stefan model on an n-sphere. By replacing the second derivative term in (1.4a) with the n-dimensional radially-symmetric Laplacian operator, Simpson [46] showed that a critical radius, R_c, governs survival and extinction analogously to the critical length. This critical radius depends on the dimension n. In the two-dimensional spreading-disc problem, the critical radius is $R_c = \alpha_{01} \approx 2.4048$, where α_{01} is the first zero of $J_0(x)$, the zeroth-order Bessel function of the first kind [46]. However, the survival and extinction behaviour of the Fisher–Stefan model remains unexplored for non-radially-symmetric two-dimensional geometries. Investigating this is the subject of our study.

2. Mathematical model

We consider a multidimensional extension to the dimensionless Fisher–Stefan model (1.4). As illustrated in Fig. 1A, we denote the region on which we solve the Fisher–KPP equation as $\Omega(t)$, and its boundary as $\partial\Omega(t)$. The boundary $\partial\Omega(t)$ defines the interface between regions of non-zero population density and regions of zero density. Biologically, this might represent the position of a cell invasion front, or the boundary of a tumour. The multidimensional Fisher–Stefan model is then

$$\frac{\partial u}{\partial t} = \nabla^2 u + u\,(1 - u), \quad \text{on} \quad \Omega(t), \tag{2.1a}$$

$$u = 0, \quad \text{on} \quad \partial\Omega(t), \tag{2.1b}$$

$$V = -\kappa \nabla u \cdot \hat{n} \quad \text{on} \quad \partial\Omega(t), \tag{2.1c}$$

$$u(x, 0) = u_0(x) \quad \text{on} \quad \Omega(0), \tag{2.1d}$$

where V is the normal speed of the interface, and $\hat{n}$ is the unit outward normal to the interface $\partial\Omega(t)$.

2.1. Numerical methods

We use the level-set method [47–51] to solve (2.1) on a two-dimensional computational domain, $\mathcal{D}$. This involves embedding the interface as the zero level-set of a scalar function $\phi(x, t)$. That is,

$$\partial\Omega(t) = \{x \mid \phi\,(x, t) = 0\}, \tag{2.2}$$

where $\phi(x, t)$ is defined for all $x \in \mathcal{D}$, and is such that $\phi < 0$ for $x \in \Omega(t)$ and $\phi \geq 0$ for $x \notin \Omega(t)$. An example for a disc is illustrated in Fig. 1B. The level-set function $\phi(x, t)$ evolves according to the level-set equation

$$\frac{\partial \phi}{\partial t} + F\,|\nabla \phi| = 0, \tag{2.3}$$

where $F(x,t)$ is the *extension velocity field*, a scalar function defined for $x \in \mathcal{D}$, such that $F = V$ on $\partial\Omega(t)$. In level-set form, the system of equations solved numerically is

$$\frac{\partial u}{\partial t} = \nabla^2 u + u(1-u) \quad \text{on} \quad \phi(x,t) < 0, \tag{2.4a}$$

$$\frac{\partial \phi}{\partial t} + F|\nabla\phi| = 0 \quad \text{on} \quad x \in \mathcal{D}, \tag{2.4b}$$

$$u = 0, \quad F = -\kappa \nabla u \cdot \frac{\nabla\phi}{|\nabla\phi|} \quad \text{on} \quad \phi(x,t) = 0, \tag{2.4c}$$

$$u(x,0) = u_0(x) \quad \text{on} \quad \phi(x,0) < 0. \tag{2.4d}$$

We solve the system (2.4) using explicit finite-difference methods [52–57]. We compute the extension velocity field by first computing V using second-order finite-differences, and then obtain F by orthogonal extrapolation [49]. An example extension velocity field for a spreading disc is shown in Fig. 1D. As ϕ evolves with time, so too does its zero level-set. This zero level-set defines the boundary of the region on which we solve (2.1a).

For each numerical solution in this work, we use 201×201 spatial resolution, with $\Delta x = \Delta y = 0.1$, $\Delta t = 0.002$, and $\kappa = 0.1$. The grid spacing and time-step sizes are sufficient to obtain good agreement with grid-independent spreading disc solutions of Simpson [46]. We choose the value $\kappa = 0.1$ to represent a slowly-expanding population, as governed by the Stefan condition (1.4d). Our choice of $\kappa = 0.1$ ensures that initially-rectangular populations remain approximately rectangular until it is clear whether the population will survive or become extinct. Full details on our level-set method, an open-source Julia implementation, and numerical tests to validate the method are available on Github. We also include documentation for our level-set method in the Supplementary Material.

3. Results and discussion

3.1. Survival and extinction in disc-shaped populations

We begin our investigation of survival and extinction in two-dimensions by considering solutions with the disc initial condition,

$$u(x,y,0) = \begin{cases} u_0 & \text{if} \quad \sqrt{\left(x-\frac{W}{2}\right)^2 + \left(y-\frac{W}{2}\right)^2} \leq R(0) \\ 0 & \text{otherwise,} \end{cases} \tag{3.1}$$

where u_0 is a constant satisfying $0 < u_0 \leq 1$, $R(0)$ is the initial disc radius, and W is the width of the square computational domain $\mathcal{D}$. Simpson [46] showed that the critical radius, $R_c = \alpha_{01} \approx 2.4048$, explains the survival and extinction behaviour of a disc. With the initial condition (3.1), the region $\Omega(t)$ evolves as a disc of radius $R(t)$. If $R(t) > R_c$ at any time, the population survives. Alternatively, if $R(t) < R_c$ for all t, then the population eventually becomes extinct. We solve the Fisher–Stefan model numerically using $u_0 = 0.5$, and compare solutions with $R(0) = 2.1$ and $R(0) = 2.4$. Although, both values of $R(0)$ are less than R_c, the Stefan-like condition (2.1c) suggests that $R(t)$ will increase for $\kappa > 0$, because $\nabla u \cdot \hat{n} < 0$ on $\partial\Omega(t)$. However, it is unclear whether $R(t)$ will ever exceed R_c, because the rate of spread V in (2.1c) depends on κ and the shape of the density profile.

Level-set numerical solutions with $R(0) = 2.1$ and $R(0) = 2.4$ are presented in Fig. 2. Panels A–D show that $R(0) = 2.1$ results in population extinction, with density $u \to 0^+$ as t increases. This is because $R(t) < R_c$ for all t, where R_c is indicated by the vertical lines in panel D. Eventually, population density $u \to 0^+$, which prevents further spread because $\nabla u \to 0$, and thus $V \to 0$ according to (2.1c). In contrast, with $R(0) = 2.4$ the population survives and spreads, such that both density u and the size of $\Omega(t)$ eventually increase with time. Although the density $u(10,10,t)$ at the centre of $\Omega(t)$ decreases at first (see panel H), we eventually have $R(t) > R_c$. This enables the density to recover, and the population to survive. As $t \to \infty$, the solution approaches a radially-symmetric travelling wave. The ability to capture both survival and extinction is an advantage of the Fisher–Stefan model over the Fisher–KPP equation.

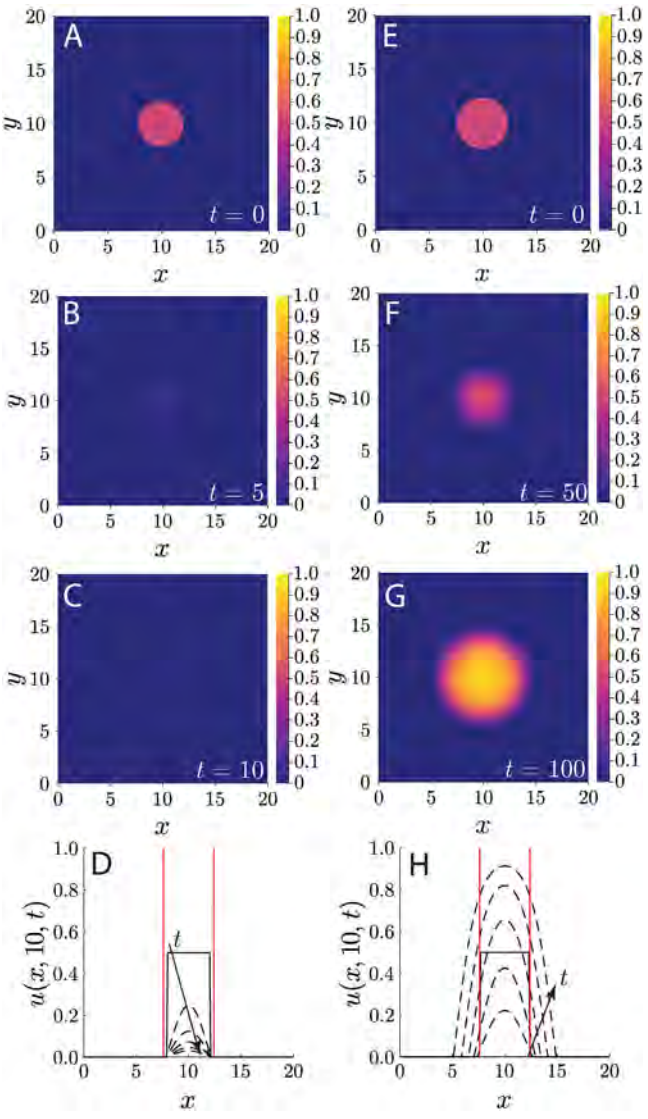

Fig. 2. Numerical solutions to the Fisher–Stefan model with the disc initial condition (3.1), and $u_0 = 0.5$. (A–D): Solution with $R(0) = 2.1$. (A): Initial condition, $t = 0$. (B): Density profile $u(x,y,t)$ at $t = 5$. (C): Density profile $u(x,y,t)$ at $t = 10$. (D): Evolution of population density, viewed as a one-dimensional slice through $y = 10$. The solid curve represents the initial condition, and dashed curves are the densities at $t \in \{2,4,6,8,10\}$. Arrow indicates direction of increasing t. (E–H): solution with $R(0) = 2.4$. (E): Initial condition, $t = 0$. (F): Density profile $u(x,y,t)$ at $t = 50$. (G): Density profile $u(x,y,t)$ at $t = 100$. (H): Evolution of population density, viewed as a one-dimensional slice through $y = 10$. The solid curve represents the initial condition, and dashed curves are the densities at $t \in \{20,40,60,80,100\}$. Arrow indicates direction of increasing t. (D&H): Red vertical line represents $x = 10 \pm R_c$, where $R_c = \alpha_{01}$.

3.2. Numerical solutions for rectangular populations

Despite being previously studied in radially-symmetric geometry, the survival and extinction behaviour of the Fisher–Stefan

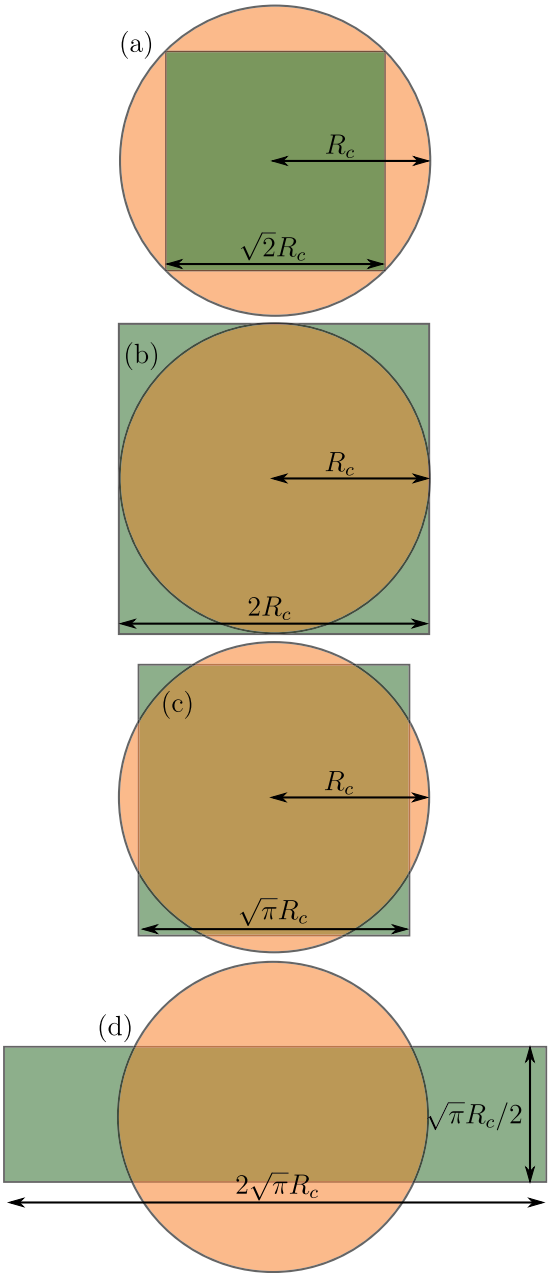

Fig. 3. Potential square and rectangular analogues to the critical disc with radius R_c. (a) A square whose corners lie on the perimeter of the circle. (b) A square with side width equal to the circle diameter. (c) A square with the same area as the circle. (d) A rectangle with aspect ratio 4, and the same area as the circle.

model in general two-dimensional geometry remains unexplored. For example, it is not immediately clear how the results for a disc translate to rectangular shapes. Given a disc of radius R_c, one can conceive many rectangles that share certain properties with the disc. Some examples are shown in Fig. 3. For example, in Fig. 3(a) we have the square with width $\sqrt{2}R_c$, for which all points inside the square are within the critical disc. In Fig. 3(b) we have the square with width $2R_c$, such that every point of the critical disc is contained within the square. Based on the radially-symmetric analysis, we would expect the initial square in Fig. 3(a) to give rise to extinction, and the initial square in Fig. 3(b) to give rise to survival. However, the situation is unclear for a square with side width between $\sqrt{2}R_c$ and $2R_c$. One example is the square with width $\sqrt{\pi}R_c$ (Fig. 3(c)), which has the same area as the critical disc. In this case, consider drawing a family of rays from the centre of the square or disc to the perimeter of each shape. Each ray is defined by its polar angle $\theta \in [0, 2\pi]$. For some θ, for example $\theta = 0, \pm\pi/2$, R_c exceeds the distance to the perimeter of the square. In contrast, for $\theta = \pm\pi/4, \pm 3\pi/4$, the distance to the perimeter of the square exceeds R_c. Therefore, it is unclear whether a population of this shape will survive or become extinct. Furthermore, varying the aspect ratio enables us to define a family of rectangles with the same area, one of which is shown in Fig. 3(d). The survival and extinction behaviour of these shapes is also unclear according to previous radially-symmetric analysis.

To address this question, we consider numerical solutions on initially-rectangular domains. We characterise the geometry of $\Omega(t)$ by defining $L_x(t)$ and $L_y(t)$ to be the distances in the x and y-directions respectively occupied by the population, measured through the centre of Ω. That is,

$$L_x(t) = \max\{x \mid u(x, W/2, t) > 0\} - \min\{x \mid u(x, W/2, t) > 0\}, \tag{3.2a}$$

$$L_y(t) = \max\{y \mid u(W/2, y, t) > 0\} - \min\{y \mid u(W/2, y, t) > 0\}. \tag{3.2b}$$

For populations that remain approximately rectangular, $L_x(t)$ and $L_y(t)$ provide measures for the rectangle width and height, respectively. For initially-rectangular domains, the initial condition is then

$$u(x, y, 0) = \begin{cases} u_0 & \text{if} \quad \left|x - \frac{W}{2}\right| \le \frac{L_x(0)}{2} \quad \text{and} \\ & \left|y - \frac{W}{2}\right| \le \frac{L_y(0)}{2}, \\ 0 & \text{otherwise.} \end{cases} \tag{3.3}$$

Fig. 4, panels (A–E) and panels (F–J) depict numerical solutions for initially-square populations. Panels A–E show that a solution with the square initial condition $L_x(0) = L_y(0) = 3.5$ leads to extinction, like the circular solution in Fig. 2, panels A–D. Increasing the size of the initial square to $L_x(0) = L_y(0) = 4$ yields survival (Fig. 4, panels F–J), similar to how increasing the initial radius led to survival in disc-shaped populations (Fig. 2, panels E–H). However, for a given κ survival or extinction of rectangular populations does not depend solely on area, unlike for disc-shaped populations. The numerical solution in Fig. 4, panels K–O confirms this. Panels K–O depict a rectangular population that becomes extinct, with initial condition $L_x(0) = 8$ and $L_y(0) = 2$. Extinction occurs despite the rectangle in panels K–O having the same initial area as the square population that survived. Thus, more detail about the region geometry than initial area is required to determine the survival or extinction of rectangular populations.

3.3. Conditions for survival and extinction in rectangular populations

To explain the results in Fig. 4, we obtain critical conditions that determine survival or extinction. Our analysis is similar to those of El-Hachem et al. [45], and Simpson [46]. It involves considering the small-density $u \to 0^+$ limit, for which the leading-order population density $\hat{u}(x, y, t)$ satisfies

$$\frac{\partial \hat{u}}{\partial t} = \frac{\partial^2 \hat{u}}{\partial x^2} + \frac{\partial^2 \hat{u}}{\partial y^2} + \hat{u}. \tag{3.4}$$

We consider solutions to (3.4) on a fixed rectangular domain $0 \le x \le X$ and $0 \le y \le Y$, subject to arbitrary compactly-supported initial conditions, and homogeneous Dirichlet boundary conditions on all boundaries. This problem has the general

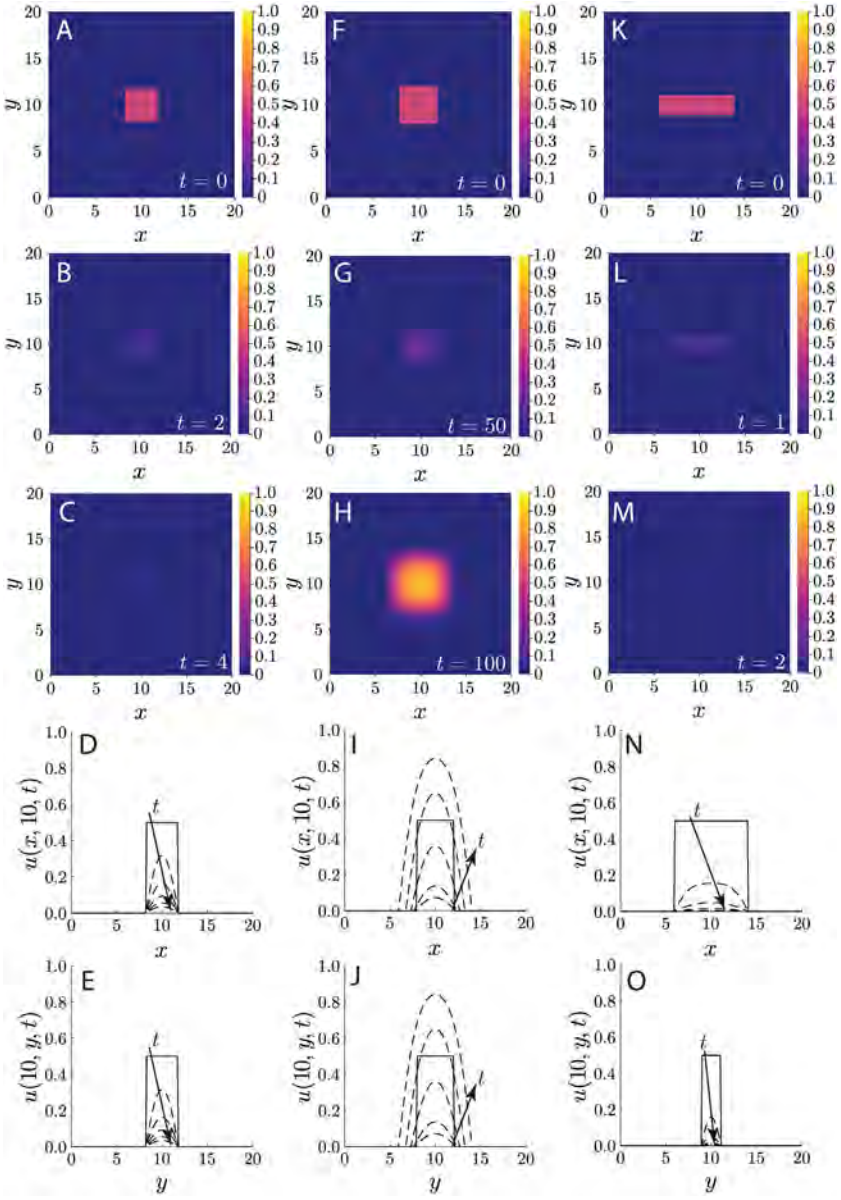

Fig. 4. Numerical solutions with rectangular initial conditions (3.3), with $u_0 = 0.5$. (A–E): Solution with $L_x(0) = L_y(0) = 3.5$. (F–J): Solution with $L_x(0) = L_y(0) = 4$. (K–O): Solution with $L_x(0) = 8$, $L_y(0) = 2$. (A): Initial density $u(x, y, 0)$. (B): Density profile at $t = 2$. (C): Density profile at $t = 4$. (D–E) One-dimensional slice $u(x, 10, t)$. $u(10, y, t)$. Solid curve is the initial condition, dashed curves are solutions plotted at $t \in \{1, 2, 3, 4, 5\}$. Arrow indicates direction of increasing t. (F): Initial density $u(x, y, 0)$. (G): Density profile at $t = 50$. (H): Density profile at $t = 100$. (I–J) One-dimensional slice $u(x, 10, t)$. $u(10, y, t)$. Solid curve is the initial condition, dashed curves are solutions plotted at $t \in \{20, 40, 60, 80, 100\}$. Arrow indicates direction of increasing t. (K): Initial density $u(x, y, 0)$. (L): Density profile at $t = 1$. (M): Density profile at $t = 2$. (N–O) One-dimensional slice $u(x, 10, t)$. $u(10, y, t)$. Solid curve is the initial condition, dashed curves are solutions plotted at $t \in \{1, 2, 3, 4, 5\}$. Arrow indicates direction of increasing t.

solution

$$\hat{u}(x, y, t) = \sum_{n=1}^{\infty}\sum_{m=1}^{\infty} A_{n,m} \sin\left(\frac{n\pi x}{X}\right) \sin\left(\frac{m\pi y}{Y}\right) \times \mathrm{e}^{-\left(\frac{n^2\pi^2}{X^2} + \frac{m^2\pi^2}{Y^2} - 1\right)t}, \tag{3.5}$$

with coefficients $A_{n,m}$ chosen such that $\hat{u}(x, y, 0)$ matches the initial condition. We next consider the long-time solution $t \to \infty$, such that the leading-eigenvalue $n = m = 1$ approximates the general solution (3.5). Then,

$$\hat{u}(x, y, t) \sim A_{1,1} \sin\left(\frac{\pi x}{X}\right) \sin\left(\frac{\pi y}{Y}\right) \mathrm{e}^{-\left(\frac{\pi^2}{X^2} + \frac{\pi^2}{Y^2} - 1\right)t} \quad \text{as} \quad t \to \infty. \tag{3.6}$$

To obtain the conditions under which the population survives or becomes extinct as $t \to \infty$, we use the approximation (3.6) and consider conservation of the population inside Ω. For $u \ll 1$, the conservation statement is

$$\frac{\mathrm{d}M}{\mathrm{d}t} = \int_{\Omega} \hat{u}(x, y, t) - \int_{\partial\Omega} -\nabla\hat{u} \cdot \hat{n}, \tag{3.7}$$

where $M(t) = \int_{\Omega} \hat{u}(x, y, t)$ is the total population in Ω. The first term on the right-hand side of (3.7) is the net accumulation of $\hat{u}$ inside Ω due to the (linearised) source term. The second term on the right-hand side of (3.7) is the rate of population loss through the boundary $\partial\Omega$ due to diffusion. The population survives if $\mathrm{d}M/\mathrm{d}t > 0$ as $t \to \infty$, that is accumulation exceeds loss. Alternatively, the population becomes extinct if $\mathrm{d}M/\mathrm{d}t < 0$ as $t \to \infty$, *i.e.* the rate of loss exceeds accumulation. Critical

behaviour occurs when $\mathrm{d}M/\mathrm{d}t = 0$ as $t \to \infty$, such that the rates of population gain and loss balance. This requires

$$\int_{\Omega} \hat{u}(x, y, t) = \int_{\partial\Omega} -\nabla\hat{u} \cdot \hat{n}. \tag{3.8}$$

In fixed rectangular geometry, Ω and $\partial\Omega$ are readily parameterised to give

$$\int_0^Y \int_0^X \hat{u}(x, y, t)\,\mathrm{d}x\,\mathrm{d}y = -\int_0^Y \frac{\partial\hat{u}(X, y, t)}{\partial x}\,\mathrm{d}y + \int_0^Y \frac{\partial\hat{u}(0, y, t)}{\partial x}\,\mathrm{d}y - \int_0^X \frac{\partial\hat{u}(x, Y, t)}{\partial y}\,\mathrm{d}x + \int_0^X \frac{\partial\hat{u}(x, 0, t)}{\partial y}\,\mathrm{d}x. \tag{3.9}$$

Substituting the leading-eigenvalue approximation (3.6) for $\hat{u}$ in (3.9), evaluating integrals, and simplifying then yields

$$XY = \pi\sqrt{Y^2 + X^2}. \tag{3.10}$$

The condition (3.10) implies that the population survives if the area XY of the rectangular region $\Omega(t)$ exceeds $\pi\sqrt{Y^2 + X^2}$. Another interpretation of the condition (3.10) is that extinction will occur if the exponential term in (3.6) decays, and the population will survive if the exponential term grows. Setting the exponent in the leading-eigenvalue approximation (3.6) to zero then yields the same condition (3.10).

The fixed-domain analysis applies to the Fisher–Stefan moving-boundary problem, provided $\Omega(t)$ remains approximately rectangular. If so, (3.10) implies that a rectangular population will survive if its lengths $L_x(t)$ and $L_y(t)$ ever satisfy $L_xL_y > \pi\sqrt{L_y^2 + L_x^2}$, and will become extinct if $L_xL_y < \pi\sqrt{L_y^2 + L_x^2}$ for all time. Another way to write the condition for survival is that the inequalities

$$L_y > \pi\sqrt{\frac{L_x^2}{L_x^2 - \pi^2}}, \quad L_x > \pi, \tag{3.11}$$

must be satisfied at some t. Interestingly, the population cannot survive if either L_x or L_y remain less than π for all time. Furthermore, for each $L_x > \pi$, there exists a unique critical $L_{y,c}$ given by the right-hand side of the first inequality in (3.11), above which the population will survive. This completely characterises the effect of rectangular geometry and aspect ratio on survival and extinction in the two-dimensional Fisher–Stefan model.

For a square-shaped population, the conditions (3.10) and (3.11) imply that survival only occurs if the square width ever exceeds $\sqrt{2}\pi \approx 4.443$. This explains the numerical results in Fig. 4, panels A–E and panels F–J. For the square solution in Fig. 4, panels A–E with $L_x(0) = L_y(0) = 3.5$, the widths never reach $\sqrt{2}\pi$, and thus the population eventually becomes extinct. However, with $L_x(0) = L_y(0) = 4$, (Fig. 4, panels F–J), the square widths do eventually exceed $\sqrt{2}\pi$, leading to eventual survival. Furthermore, although the rectangle with $L_x(0) = 8$ and $L_y(0) = 2$ has the same initial area as the square with $L_x(0) = L_y(0) = 4$, the population becomes extinct because $L_y(t) < \pi$ for all t, which guarantees extinction according to (3.11).

Fig. 5 illustrates how some numerical solutions with rectangular initial conditions evolve. These solutions include the three solutions from Fig. 4, and solutions with $(L_x(0), L_y(0)) \in \{(10, 2.5), (8, 3), (6, 4)\}$. If the inequalities (3.11) hold for any t, the population survives and L_x and L_y continue to increase. This is shown by the trajectories above the red curve in Fig. 5. Conversely, the population becomes extinct if (3.11) never holds. This occurs for the trajectories that remain below the red curve in Fig. 5.

The critical conditions (3.11) are valid if the domain $\Omega(t)$ remains approximately rectangular. Our choice of $\kappa = 0.1$ in all numerical solutions of Figs. 4 and 5 ensures that the rectangular shapes persist sufficiently long for (3.11) to determine survival or extinction. With much larger κ, for example $\kappa = 1$, initially-rectangular shapes satisfying the survival conditions evolve to an expanding disc. In these scenarios, the long-term survival-extinction behaviour instead obeys the critical radius condition of Simpson [46].

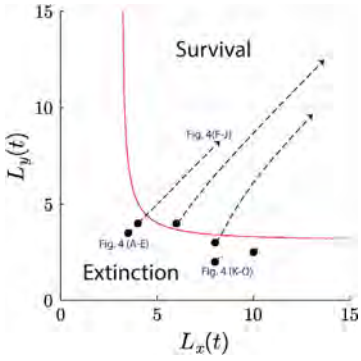

Fig. 5. Evolution of numerical solutions to the Fisher–Stefan model with rectangular initial conditions. Black dots represent the initial rectangle dimensions $L_x(0)$, and $L_y(0)$ for each solution plotted. Dashed curves represent the evolution of $L_x(t)$ and $L_y(t)$ from $t = 0$ to $t = 10$ for extinction solutions, or $t = 0$ to $t = 100$ for survival solutions. The red curve defines the critical threshold between survival and extinction, as per (3.11). Solutions corresponding to panels (A–E), panels (F–J), and panels (K–O) of Fig. 4 are labelled.

4. Conclusion and future work

The Fisher–Stefan model provides an alternative to standard the Fisher–KPP model that both defines an unambiguous invasion front, and admits solutions whereby the population becomes extinct. In this study, we extended one-dimensional and radially-symmetric results for the Fisher–Stefan model to two-dimensional rectangular domains. Using the level-set method, we computed numerical solutions to the two-dimensional Fisher–Stefan model with $\kappa = 0.1$, for radially-symmetric and rectangular domains. Our objective was to understand the conditions under which square and rectangular shapes give rise to survival or extinction.

To explain the numerical observations, we obtained conditions for the Fisher–Stefan model that govern survival and extinction of a rectangular-shaped population. Using a conservation argument in the small density limit, we showed that survival requires both lengths of the rectangle to exceed π, and for the rectangle area to exceed a critical threshold that depends on the side lengths. Extending the one-dimensional idea of critical length or critical radius to a critical area in two dimensions is insufficient to explain survival and extinction. Instead, for rectangular-shaped domains information about both widths is necessary. Interestingly, these findings are similar to the behaviour of a population subject to the strong Allee effect. In radially-symmetric geometry, Lewis and Kareiva [58] showed that a critical radius governs survival and extinction. However, recent work by Li et al. [59] showed that additional geometric information is required to determine survival or extinction in asymmetric two-dimensional rectangular domains.

The analytical methods established in this work apply directly to any domain $\Omega(0)$ such that solution to (3.4) with homogeneous Dirichlet conditions on $\partial\Omega(0)$ can be obtained using separation of variables. One avenue for future work is to investigate the conditions for survival and extinction in these separable shapes, for example an ellipse [60]. Furthermore, our numerical method can be used to study survival and extinction for

general initial shapes $\Omega(0)$, regardless of whether these are separable. This includes investigation of non-simply-connected initial shapes. Furthermore, the analytical and numerical techniques can be extended to general reaction–diffusion moving-boundary problems. One possibility is to replace the Fisher–KPP equation with a nonlinear degenerate diffusion equation, for example (1.2), with $D(u) = u^k$, for some $k > 0$ [25]. We do not investigate nonlinear diffusion here, because linear diffusion is the most common assumption for biological dispersal in reaction–diffusion equations. Furthermore, in nonlinear degenerate diffusion models k is an additional parameter to be estimated, and the biological or ecological interpretation of k remains unclear [13].

All numerical solutions presented in this work have $\kappa = 0.1$. When solving the Fisher–Stefan model numerically with much larger κ, for example $\kappa = 1$, we observed that initially square and rectangular domains that satisfied the conditions for survival quickly evolved to an expanding circular shape. This numerical evidence suggests that radially-symmetric survival solutions to the Fisher–Stefan model are stable with respect to small-amplitude azimuthal perturbations. However, this has not been verified analytically. The stability of inward-moving fronts in a hole-closing geometry [21] is also yet to be analysed. We plan to investigate this stability problem using analytical and numerical methods in future work.

CRediT authorship contribution statement

Alexander K.Y. Tam: Wrote the numerical code, Obtained the results, Performed the analysis, Wrote the manuscript. **Matthew J. Simpson:** Designed the research, Wrote the numerical code, Obtained the results, Performed the analysis, Wrote the manuscript.

Declaration of competing interest

The authors declare that they have no known competing financial interests or personal relationships that could have appeared to influence the work reported in this paper.

Acknowledgements

Computational resources and services used in this work were provided by HPC and Research Support Group, Queensland University of Technology, Brisbane, Australia. M. J. S. also acknowledges funding from the Australian Research Council (Grant No. DP200100177). We thank two anonymous referees for their helpful comments.

Appendix A. Supplementary data

Supplementary material related to this article can be found online at https://doi.org/10.1016/j.physd.2022.133305.

References

[1] A. Kolmogorov, I. Petrovsky, N. Piskunov, A study of the equation of diffusion with increase in the quantity of matter, and its application to a biological problem, Bull. Moscow State Univ. A 1 (1937) 1–25.
[2] J. Canosa, On a nonlinear diffusion equation describing population growth, IBM J. Res. Dev. 17 (4) (1973) 307–313, http://dx.doi.org/10.1147/rd.174.0307.
[3] P. Grindrod, Patterns and Waves: The Theory and Applications of Reaction–Diffusion Equations, Oxford University Press, 1991.
[4] J.D. Murray, Mathematical Biology I: An Introduction, third ed., Springer, 2002, http://dx.doi.org/10.1007/b98868.
[5] B.H. Bradshaw-Hajek, P. Broadbridge, A robust cubic reaction–diffusion system for gene propagation, Math. Comput. Modelling 39 (9) (2004) 1151–1163, http://dx.doi.org/10.1016/S0895-7177(04)90537-7.
[6] J.G. Skellam, Random dispersal in theoretical populations, Biometrika 38 (1–2) (1951) 196–218, http://dx.doi.org/10.1093/biomet/38.1-2.196.
[7] N. Shigesada, K. Kawasaki, Y. Takeda, Modeling stratified diffusion in biological invasions, Amer. Nat. 146 (2) (1995) 229–251, http://dx.doi.org/10.1086/285796.
[8] P. Broadbridge, A.J. Hutchinson, Integrable nonlinear reaction-diffusion population models for fisheries, Appl. Math. Model. 102 (2022) 748–767, http://dx.doi.org/10.1016/j.apm.2021.10.013.
[9] G.N. Mercer, R.O. Weber, Combustion wave speed, Proc. R. Soc. A 450 (1938) (1995) 193–198, http://dx.doi.org/10.1098/rspa.1995.0079.
[10] R.A. Gatenby, E.T. Gawlinski, A reaction–diffusion model of cancer invasion, Cancer Res. 56 (24) (1996) 5745–5753.
[11] P.K. Maini, D.L.S. McElwain, D.I. Leavesley, Traveling wave model to interpret a wound-healing cell migration assay for human peritoneal mesothelial cells, Tissue Eng. 10 (3–4) (2004) 475–482, http://dx.doi.org/10.1089/107632704323061834.
[12] B.G. Sengers, C.P. Please, R.O.C. Oreffo, Experimental characterization and computational modelling of two-dimensional cell spreading for skeletal regeneration, J. R. Soc. Interface 4 (17) (2007) 1107–1117, http://dx.doi.org/10.1098/rsif.2007.0233.
[13] J.A. Sherratt, J.D. Murray, Models of epidermal wound healing, Proc. R. Soc. B 241 (1300) (1990) 29–36, http://dx.doi.org/10.1098/rspb.1990.0061.
[14] M.J. Simpson, K.K. Treloar, B.J. Binder, P. Haridas, K.J. Manton, D.I. Leavesley, D.L.S. McElwain, R.E. Baker, Quantifying the roles of cell motility and cell proliferation in a circular barrier assay, J. R. Soc. Interface 10 (82) (2013) 20130007, http://dx.doi.org/10.1098/rsif.2013.0007.
[15] K.K. Treloar, M.J. Simpson, D.L.S. McElwain, R.E. Baker, Are *in Vitro* estimates of cell diffusivity and cell proliferation rate sensitive to assay geometry? J. Theoret. Biol. 356 (2014) 71–84, http://dx.doi.org/10.1016/j.jtbi.2014.04.026.
[16] S.T. Johnston, E.T. Shah, L.K. Chopin, D.L.S. McElwain, M.J. Simpson, Estimating cell diffusivity and cell proliferation rate by interpreting IncuCyte ZOOM™ assay data using the Fisher–Kolmogorov model, BMC Syst. Biol. 9 (1) (2015) 38, http://dx.doi.org/10.1186/s12918-015-0182-y.
[17] M. El-Hachem, S.W. McCue, M.J. Simpson, Invading and receding sharp-fronted travelling waves, Bull. Math. Biol. 83 (4) (2021) 35, http://dx.doi.org/10.1007/s11538-021-00862-y.
[18] K.A. Landman, G.J. Pettet, D.F. Newgreen, Mathematical models of cell colonization of uniformly growing domains, Bull. Math. Biol. 65 (2) (2003) 235–262, http://dx.doi.org/10.1016/S0092-8240(02)00098-8.
[19] K.R. Swanson, C. Bridge, J.D. Murray, E.C. Alvord Jr., Virtual and real brain tumors: Using mathematical modeling to quantify glioma growth and invasion, J. Neurol. Sci. 216 (1) (2003) 1–10, http://dx.doi.org/10.1016/j.jns.2003.06.001.
[20] V.M. Pérez-García, G.F. Calvo, J. Belmonte-Beitia, D. Diego, L. Pérez-Romasanta, Bright solitary waves in malignant gliomas, Phys. Rev. E 84 (2) (2011) 021921, http://dx.doi.org/10.1103/PhysRevE.84.021921.
[21] S.W. McCue, W. Jin, T.J. Moroney, K. Lo, S. Chou, M.J. Simpson, Hole-closing model reveals exponents for nonlinear degenerate diffusivity functions in cell biology, Physica D 398 (2019) 130–140, http://dx.doi.org/10.1016/j.physd.2019.06.005.
[22] T.P. Witelski, Merging traveling waves for the Porous-Fisher's equation, Appl. Math. Lett. 8 (4) (1995) 57–62, http://dx.doi.org/10.1016/0893-9659(95)00047-T.
[23] W.S.C. Gurney, R.M. Nisbet, The regulation of inhomogeneous populations, J. Theoret. Biol. 52 (2) (1975) 441–457, http://dx.doi.org/10.1016/0022-5193(75)90011-9.
[24] D.J. Warne, R.E. Baker, M.J. Simpson, Using experimental data and information criteria to guide model selection for reaction–diffusion problems in mathematical biology, Bull. Math. Biol. 81 (6) (2019) 1760–1804, http://dx.doi.org/10.1007/s11538-019-00589-x.
[25] F. Sánchez-Garduño, P.K. Maini, Existence and uniqueness of a sharp travelling wave in degenerate non-linear diffusion Fisher-KPP equations, J. Math. Biol. 33 (2) (1994) 163–192, http://dx.doi.org/10.1007/BF00160178.
[26] J.A. Sherratt, B.P. Marchant, Nonsharp travelling wave fronts in the Fisher equation with degenerate nonlinear diffusion, Appl. Math. Lett. 9 (5) (1996) 33–38, http://dx.doi.org/10.1016/0893-9659(96)00069-9.
[27] S.L. Mitchell, M. Vynnycky, Finite-difference methods with increased accuracy and correct initialization for one-dimensional Stefan problems, Appl. Math. Comput. 215 (4) (2009) 1609–1621, http://dx.doi.org/10.1016/j.amc.2009.07.054.
[28] S.L. Mitchell, T.G. Myers, Improving the accuracy of heat balance integral methods applied to thermal problems with time dependent boundary conditions, Int. J. Heat Mass Transfer 53 (17) (2010) 3540–3551, http://dx.doi.org/10.1016/j.ijheatmasstransfer.2010.04.015.
[29] M.P. Dalwadi, S.L. Waters, H.M. Byrne, I.J. Hewitt, A mathematical framework for developing freezing protocols in the cryopreservation of cells, SIAM J. Appl. Math. 80 (2) (2020) 657–689, http://dx.doi.org/10.1137/19M1275875.
[30] F. Brosa Planella, C.P. Please, R.A. Van Gorder, Extended Stefan problem for solidification of binary alloys in a finite planar domain, SIAM J. Appl. Math. 79 (3) (2019) 876–913, http://dx.doi.org/10.1137/18M118699X.

[31] F. Brosa Planella, C.P. Please, R.A. Gorder, Extended Stefan problem for the solidification of binary alloys in a sphere, European J. Appl. Math. 32 (2) (2021) 242–279, http://dx.doi.org/10.1017/S095679252000011X.
[32] J. Crank, Free and Moving Boundary Problems, Oxford University Press, 1987.
[33] R. Shuttleworth, D. Trucu, Multiscale modelling of fibres dynamics and cell adhesion within moving boundary cancer invasion, Bull. Math. Biol. 81 (7) (2019) 2176–2219, http://dx.doi.org/10.1007/s11538-019-00598-w.
[34] L.S. Kimpton, J.P. Whiteley, S.L. Waters, J.R. King, J.M. Oliver, Multiple travelling-wave solutions in a minimal model for cell motility, Math. Med. Biol. 30 (3) (2013) 241–272, http://dx.doi.org/10.1093/imammb/dqs023.
[35] N.T. Fadai, M.J. Simpson, New travelling wave solutions of the Porous–Fisher model with a moving boundary, J. Phys. A 53 (9) (2020) 095601, http://dx.doi.org/10.1088/1751-8121/ab6d3c.
[36] E.A. Gaffney, P.K. Maini, C.D. McCaig, M. Zhao, J.V. Forrester, Modelling corneal epithelial wound closure in the presence of physiological electric fields via a moving boundary formalism, Math. Med. Biol.: J. IMA 16 (4) (1999) 369–393, http://dx.doi.org/10.1093/imammb/16.4.369.
[37] J.P. Ward, J.R. King, Mathematical modelling of avascular-tumour growth, Math. Med. Biol.: J. IMA 14 (1) (1997) 39–69, http://dx.doi.org/10.1093/imammb/14.1.39.
[38] M. Basiri, F. Lutscher, A. Moameni, The existence of solutions for a free boundary problem modeling the spread of ecosystem engineers, J. Nonlinear Sci. 31 (5) (2021) 72, http://dx.doi.org/10.1007/s00332-021-09725-1.
[39] K.P. Hadeler, Stefan problem, traveling fronts, and epidemic spread, Discrete Contin. Dyn. Syst. – B 21 (2) (2016) 417, http://dx.doi.org/10.3934/dcdsb.2016.21.417.
[40] N.T. Fadai, Semi-infinite travelling waves arising in a general reaction–diffusion Stefan model, Nonlinearity 34 (2) (2021) 725–743, http://dx.doi.org/10.1088/1361-6544/abd07b.
[41] Y. Du, Z. Lin, Spreading–vanishing dichotomy in the diffusive logistic model with a free boundary, SIAM J. Math. Anal. 42 (1) (2010) 377–405, http://dx.doi.org/10.1137/090771089.
[42] Y. Du, Z. Guo, Spreading–vanishing dichotomy in a diffusive logistic model with a free boundary, II, J. Differential Equations 250 (12) (2011) 4336–4366, http://dx.doi.org/10.1016/j.jde.2011.02.011.
[43] Y. Du, Z. Guo, The Stefan problem for the Fisher–KPP equation, J. Differential Equations 253 (3) (2012) 996–1035, http://dx.doi.org/10.1016/j.jde.2012.04.014.
[44] S.W. McCue, M. El-Hachem, M.J. Simpson, Exact sharp-fronted travelling wave solutions of the Fisher–KPP equation, Appl. Math. Lett. 114 (2021) 106918, http://dx.doi.org/10.1016/j.aml.2020.106918.
[45] M. El-Hachem, S.W. McCue, W. Jin, Y. Du, M.J. Simpson, Revisiting the Fisher–Kolmogorov–Petrovsky–Piskunov equation to interpret the spreading–extinction dichotomy, Proc. R. Soc. A 475 (2229) (2019) 20190378, http://dx.doi.org/10.1098/rspa.2019.0378.
[46] M.J. Simpson, Critical length for the spreading–Vanishing dichotomy in higher dimensions, ANZIAM J. 62 (1) (2020) 3–17, http://dx.doi.org/10.1017/S1446181120000103.
[47] S. Osher, J.A. Sethian, Fronts propagating with curvature-dependent speed: Algorithms based on Hamilton-Jacobi formulations, J. Comput. Phys. 79 (1) (1988) 12–49, http://dx.doi.org/10.1016/0021-9991(88)90002-2.
[48] J.A. Sethian, Level Set Methods and Fast Marching Methods: Evolving Interfaces in Computational Geometry, Fluid Mechanics, Computer Vision, and Materials Science, second ed., in: Cambridge Monographs on Applied and Computational Mathematics, Cambridge University Press, 32 Avenue of the Americas, New York, NY 10013-2473, USA, 1999.
[49] S. Osher, R.P. Fedkiw, Level Set Methods and Dynamic Implicit Surfaces, in: Applied Mathematical Sciences, Springer-Verlag, New York, 2003.
[50] T.D. Aslam, A partial differential equation approach to multidimensional extrapolation, J. Comput. Phys. 193 (1) (2004) 349–355, http://dx.doi.org/10.1016/j.jcp.2003.08.001.
[51] L.C. Morrow, T.J. Moroney, M.C. Dallaston, S.W. McCue, A review of one-phase Hele-Shaw flows and a level-set method for nonstandard configurations, ANZIAM J. 63 (3) (2021) 269–307, http://dx.doi.org/10.1017/S144618112100033X.
[52] C. Tsitouras, Runge–Kutta pairs of order 5(4) satisfying only the first column simplifying assumption, Comput. Math. Appl. 62 (2) (2011) 770–775, http://dx.doi.org/10.1016/j.camwa.2011.06.002.
[53] C.V. Rackauckas, Q. Nie, Differentialequations.Jl – A performant and feature-rich ecosystem for solving differential equations in Julia, J. Open Res. Softw. 5 (1) (2017) 15, http://dx.doi.org/10.5334/jors.151.
[54] C.T. Lin, E. Tadmor, High-resolution nonoscillatory central schemes for Hamilton–Jacobi equations, SIAM J. Sci. Comput. 21 (6) (2000) 2163–2186, http://dx.doi.org/10.1137/S1064827598344856.
[55] G.S. Jiang, D. Levy, C.T. Lin, S. Osher, E. Tadmor, High-resolution nonoscillatory central schemes with nonstaggered grids for hyperbolic conservation laws, SIAM J. Numer. Anal. 35 (6) (1998) 2147–2168, http://dx.doi.org/10.1137/S0036142997317560.
[56] H. Nessyahu, E. Tadmor, Non-oscillatory central differencing for hyperbolic conservation laws, J. Comput. Phys. 87 (2) (1990) 408–463, http://dx.doi.org/10.1016/0021-9991(90)90260-8.
[57] M.J. Simpson, K.A. Landman, T.P. Clement, Assessment of a non-traditional operator split algorithm for simulation of reactive transport, Math. Comput. Simulation 70 (1) (2005) 44–60, http://dx.doi.org/10.1016/j.matcom.2005.03.019.
[58] M.A. Lewis, P. Kareiva, Allee dynamics and the spread of invading organisms, Theor. Popul. Biol. 43 (2) (1993) 141–158, http://dx.doi.org/10.1006/tpbi.1993.1007.
[59] Y. Li, S.T. Johnston, P.R. Buenzli, P. van Heijster, M.J. Simpson, Extinction of bistable populations is affected by the shape of their initial spatial distribution, Bull. Math. Biol. 84 (1) (2021) 21, http://dx.doi.org/10.1007/s11538-021-00974-5.
[60] M. Abramowitz, I.A. Stegun, Handbook of Mathematical Functions with Formulas, Graphs, and Mathematical Tables, tenth ed., in: Applied Mathematics Series, United States Department of Commerce, National Bureau of Standards; Dover Publications, Washington, D. C., 1964.